IOP Conference Series: Materials Science and Engineering

Structural design and simulation analysis of the carbon fiber-reinforced polymer main frame of a mapping camera system

To cite this article: Q L Wang *et al* 2019 *IOP Conf. Ser.: Mater. Sci. Eng.* **474** 012031

IOP Conf. Series: Materials Science and Engineering 474 (2019) 012031 doi:10.1088/1757-899X/474/1/012031

Structural design and simulation analysis of the carbon fiber-reinforced polymer main frame of a mapping camera system

Q L Wang*, W Z Wang, Q X Wang, H J Jiang, X H Zhou, and L Zhang

Beijing Institute of Space Mechanics & Electricity, China.

*E-mail: 13488723514@163.com

Abstract. The main frame is the primary load-bearing component of a mapping camera system. As the critical structure of the system, the main frame determines the mechanical properties of a camera system. The main frame design is hindered by its large size, complicated interface, as well as high-stability, high-frequency requirement, and lightweight requirements. During the launching process, the main frame should be able to withstand the mechanical action of the active section without affecting the performance of the camera system. This paper describes the design scheme of the main frame. The modal analysis, static analysis and frequency response analysis of the main frame are performed. The simulation analysis results prove that the natural frequency of the mapping camera system satisfies the design requirements and the main frame satisfies the required safety margin in the linear overload in X-, Y-, and Z-directions. Moreover, under condition of the frequency response in X-, Y-, and Z-directions, the main frame has excellent structural stiffness, which provides a proper mechanical environment for the camera system. The design scheme of the main frame is reasonable and feasible.

1. Introduction

The mapping camera is an integral part of the remote sensor for ground imaging observation. From the original film recoverable camera to the present transmission camera and from the frame type camera to the single-linear array, two-linear array, and three-linear CCD camera, the spatial resolution is reduced from tens of meters to 0.3m [1-2]. The two-linear array stereo mapping camera is the main load of the surveying satellite. It is composed of a front camera, a rear camera, and a main frame. The combination of the laser range finder and stereo mapping camera can obtain high accuracy of 3D positioning of ground targets [3]. The mapping camera system is installed on the satellite platform through the main frame [4].

During the launching process, the main frame should be able to withstand the mechanical action of the active section without affecting the performance of the camera system. In orbit operation, the main frame should maintain the stability of the angle of the mapping camera under the condition of a given temperature environment. The main frame should also avoid the influence of the structural deformation caused by the thermal environment factors on the geometric relationship between the mapping cameras [5].

To sum up, the main frame is the primary load-bearing component of a mapping camera system. As the key element of the system, the main frame controls the mechanical properties of the camera system. [6-7]. Combining the advantages of high specific stiffness, low density and low expansion coefficient of carbon fiber composites [8-10], the design scheme of a carbon fiber-reinforced polymer main frame is presented. To obtain a high stability composite material system main frame, the modal

IOP Conf. Series: Materials Science and Engineering 474 (2019) 012031 doi:10.1088/1757-899X/474/1/012031

analysis, static analysis, and frequency response analysis of the main frame is carried out.

2. Structural topology optimization design

2.1. Structural topology optimization theory

The purpose of structural topology optimization is to optimize certain properties of the structure or to reduce its weight by seeking the structural stiffness in the optimal distribution of the design space or to find the best way of structural force transmission path [11].

The material equivalent elastic modulus based on the variable density method can be expressed as in [12]:

$$E_p(x_i) = E_{\min} + f(x_i, p)(E_0 - E_{\min}) \tag{1}$$

Assume that

$$\Delta E = E_0 - E_{\min}$$

Then, Equation (1) can be expressed as

$$E_p(x_i) = E_{\min} + f(x_i, p)\Delta E \tag{2}$$

In Equation (2), ΔE is the equivalent elastic modulus after interpolation, E_0 is the elastic modulus of the solid material, $E_{\min}$ is the elastic modulus of the material of the hole portion, $f(x_i, p)$ is the density interpolation function. If the relative density of the ***i***-th unit is 1, it means that the unit is a solid material, and if the relative density is 0, it is represented as space.

2.2. Structural topology optimization design

The topology optimization of the structure uses the Optistruct module of the Hypermesh software package. The constraint boundaries are as follows:

1) The main frame has an analog load, and the bottom plate mounting point is fixedly installed;
2) Optimization method: variable density method;
3) Optimization constraints: camera fundamental frequency exceeds 22Hz;
4) Optimization goal: The quality of the main frame is the smallest.

Through the topology optimization of the main frame, the main force path and topology configuration are obtained, as shown in figure 1.

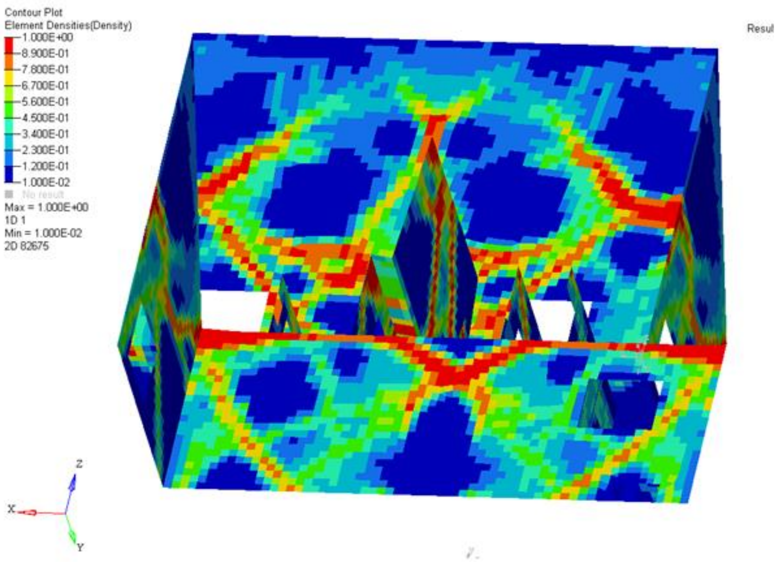

Figure 1. Optimization result for the main frame

According to the results of topology optimization, the main frame is lightweight, and the position of the ribs is reasonably arranged, which significantly reduces the structure weight. The main frame is shown in figure 2. The main frame adopts the box structure design idea, which is composed of carbon fiber composite honeycomb panels, and the inside of the honeycomb panel is provided with reinforcing ribs according to the force transmission path.

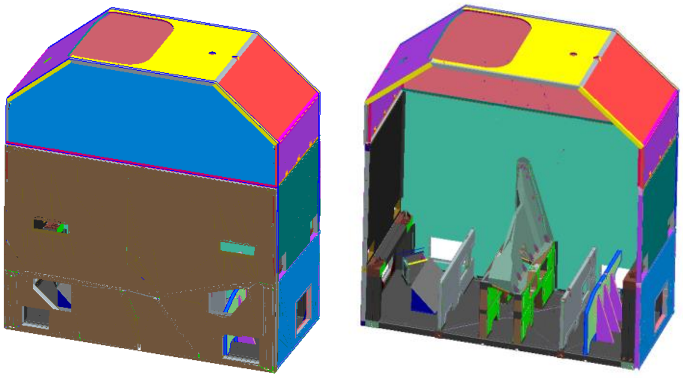

Figure 2. Schematic diagram of the main frame

3. Modal analysis

Modal analysis is used to derive the natural frequency and vibration mode of the mapping camera system. It is an integral part of the mapping camera system research process [13]. Through modal analysis, the inherent vibration mode of the surveying camera system can be obtained. The weak link of the stiffness of the main frame can also be determined, which can verify the rationality of its structural design and improve the design effectively.

3.1. Finite element modeling

According to the design requirements, it is necessary to calculate the fundamental frequency of the two stereo mapping cameras and the laser range finder under the condition of the mapping camera system. The modeling of the mapping camera system is completed in hyper mesh, in which the front and Rear cameras are modeled in detail according to the design results, and the laser range finder uses the quality point to simplify the modeling. The main frame of the system is modeled by shell element, solid element, and beam element. The finite element model of the surveying camera system is shown in figure 3.

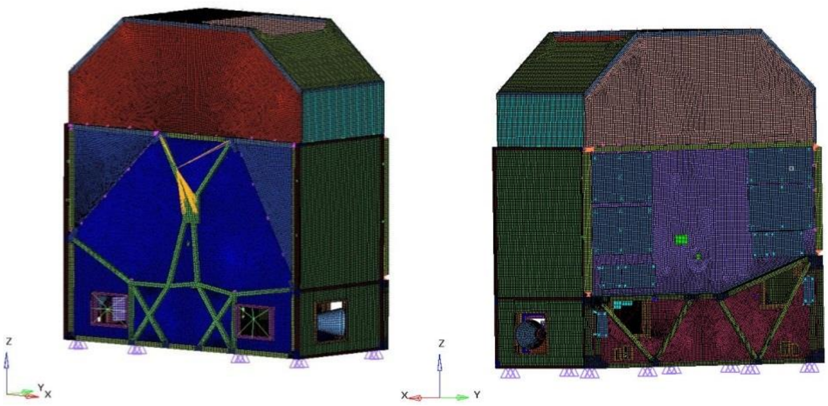

Figure 3. Finite element model of the mapping camera system

3.2. Modal analysis

According to the installation constraints of the surveying camera system, a total of 32 installation points in the eight groups of the main frame are fixed, and the modal analysis is completed. The third- and fourth-order modal analysis results are shown in figure 4.

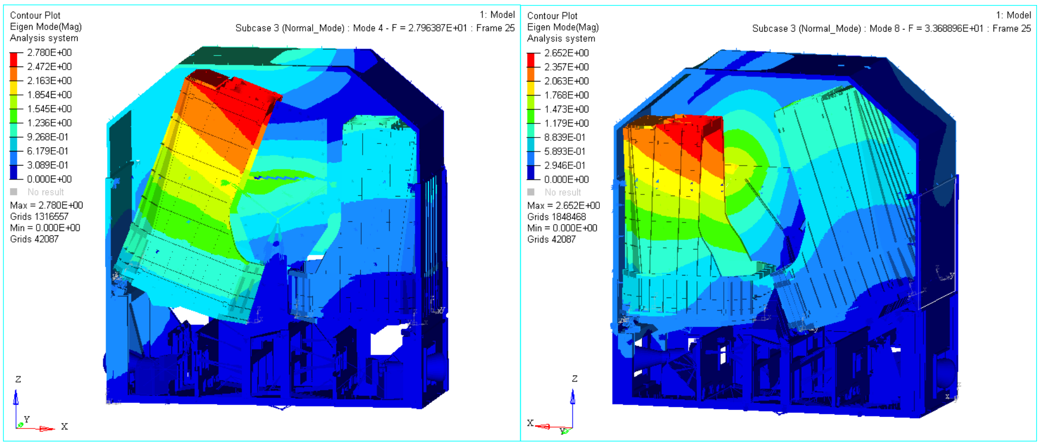

a) third-order mode front camera at 28Hz b) fourth-order mode rear camera at 33.5Hz

Figure 4. Model analysis of the mapping camera system

The result of the modal analysis shows that under the constraint conditions of the mapping camera system, the base frequencies of the front and rear cameras are 28 and 30.4Hz, respectively, which meets the requirements of no less than 25Hz in the assignment document.

4. Static Analysis

4.1. Finite element modeling

To accurately analyze the mechanical properties of all parts of the main frame, the front and rear cameras, and the laser range finder are calculated by the simplified model of the mass point. The finite element model of the mapping camera system is shown in figure 5.

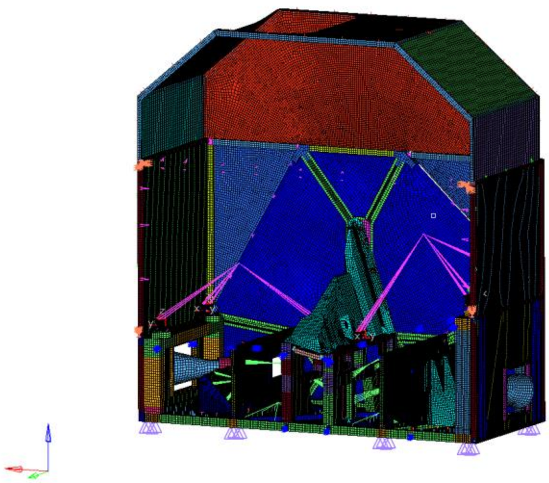

Figure 5. Finite element model of the mapping camera system.

4.2. *Static analysis*

4.2.1. *X-direction 3g linear overload.*

The calculation results of X-direction 3g linear overload are shown in figure 6. The maximum stress of the titanium alloy joint is 87.9MPa, which is located at the central support point of the front and rear cameras. The maximum value of the failure factor of the composite material is 0.07, which is located at the installation point of the main frame and satellite platform.

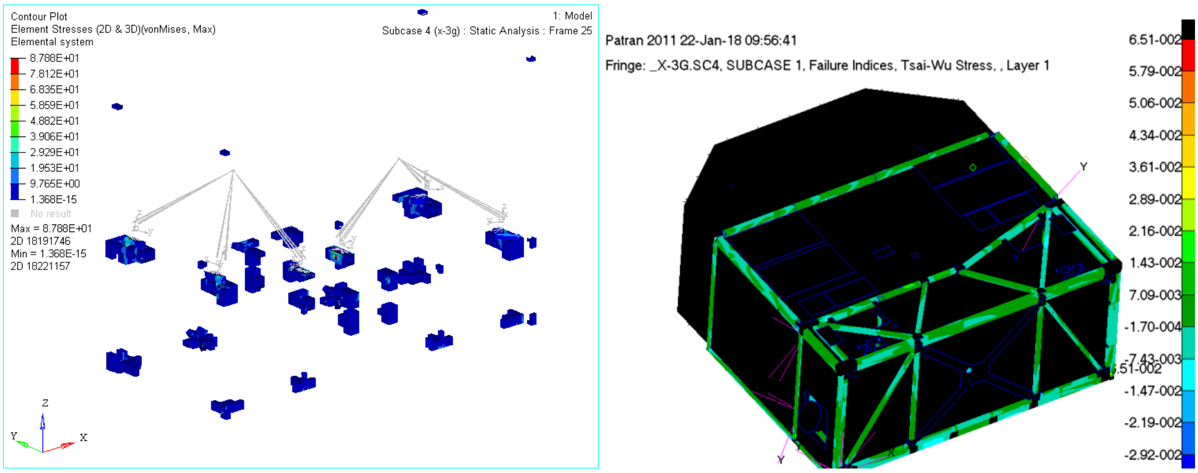

Figure 6. Cloud chart of stress distribution in titanium alloy joints and composite material failure indices by the Tsai-Wu criterion

4.2.2. *3g linear overload in Y-direction.*

The calculation results of 3g linear overload in Y-direction are shown in figure 7. The maximum stress of the titanium alloy joint is 78.7MPa, which is located at the central joint of the +Y side honeycomb plate. The maximum value of the failure index of the composite material is 0.11, which is located at the installation point of the main frame and satellite platform.

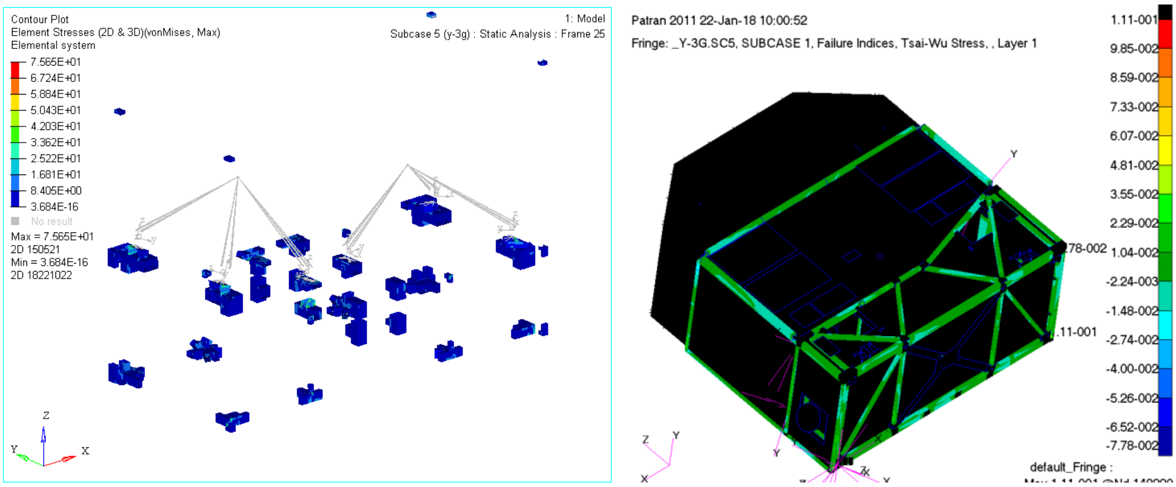

Figure 7. Cloud chart of stress distribution in titanium alloy joints and composite material indices by the Tsai-Wu criterion

4.2.3. 8g linear overload in Z-direction.
The calculation results of 8g linear overload in Z-direction are shown in figure 8. The maximum stress of the titanium alloy joint is 98MPa, which is located at the central joint of the +Y side honeycomb plate. The maximum value of the failure index of the composite material is 0.11, which is located at the installation point of the main frame and satellite platform.

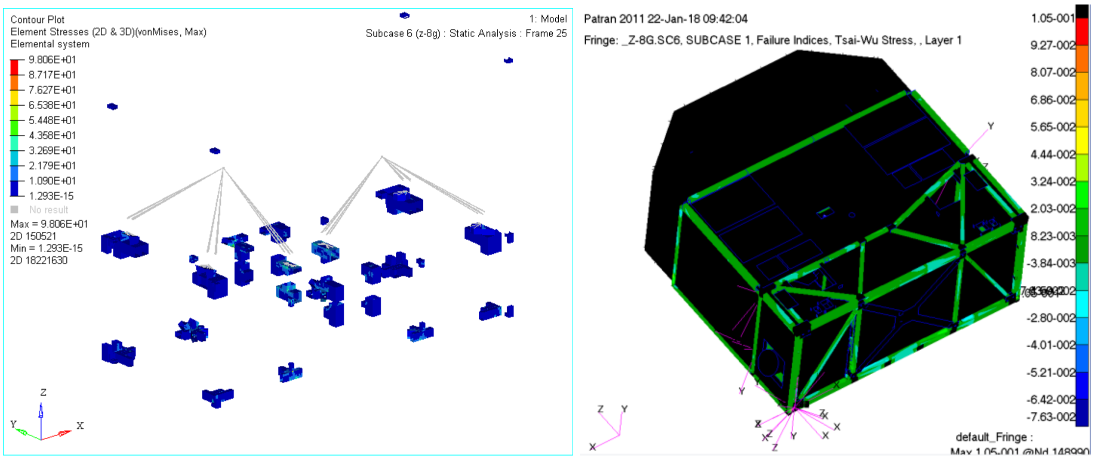

Figure 8. Cloud chart of stress distribution in titanium alloy joints and composite material failure indices by the Tsai-Wu criterion

5. Frequency response analysis

5.1. Analysis of X-direction sinusoidal response
The analysis result of X-direction sinusoidal response is shown in figure 9, where the following patterns can be observed.
1) The monitoring points with response exceeding 10g are mainly the centroid of the laser range finder and rear cameras, which are 16g@30Hz and 23g@40Hz, respectively.
2) The response of the centroid of the front and Rear cameras is amplified three times and eight times respectively. It shows that the structure of the main frame is very rigid, and it can provide an excellent mechanical environment for the mapping camera system.
3) The response of the centroid of the laser range finder is 17 times higher. Considering that the input point of laser range finder is smaller, it can meet the requirements of the mechanical environment.
4) The response of the centroid of the two stereo mapping cameras and the laser range finder is not much different from that of their input surface.

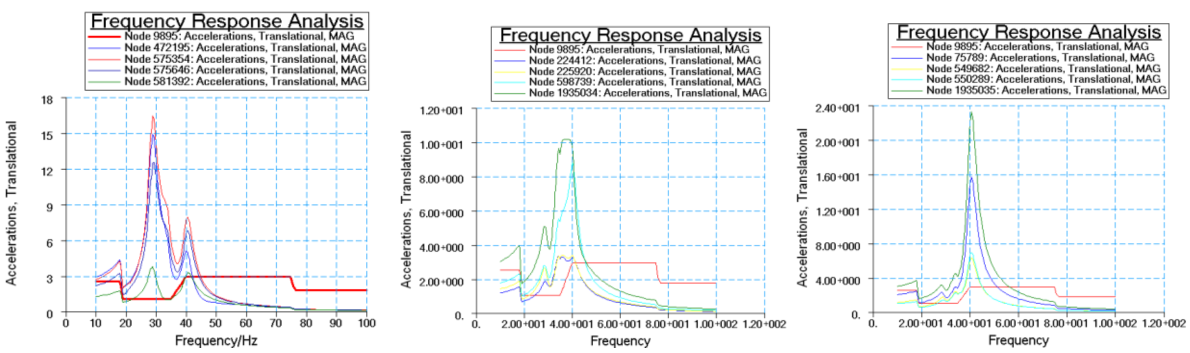

(a)Laser range finder (b) Front camera (c) Rear camera

Figure 9. X-direction sinusoidal response cures

5.2. Analysis of Y-direction sinusoidal response

The analysis result of Y-direction sinusoidal response is shown in figure 10, where the following patterns can be observed.

1) The monitoring points with larger response are mainly the centroid of the laser range finder and the front and Rear cameras.

2) The responses of the centroid of the front and rear cameras are 13g@28Hz and 24g@38Hz, respectively. Because the response of the camera's centroid is less than 30g, the stereo mapping cameras can meet the requirements of the resistance environment.

3) The response of the centroid of the laser range finder is 26g@20Hz. The peak response of the laser range finder is about 16 times higher than its input surface. Considering that the input point of laser range finder is smaller, the laser range finder has better mechanical conditions.

4) The response of the centroid of the two stereo mapping cameras and the laser range finder is not much different from that of their input surface.

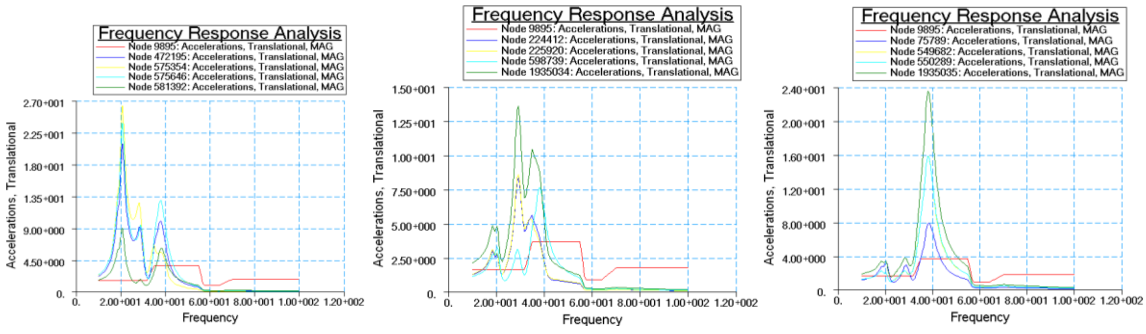

(a)Laser range finder (b) Front camera (c) Rear camera

Figure 10. Y-direction sinusoidal response cures

5.3. Analysis of Z-direction sinusoidal response

The analysis result of Z-direction sinusoidal response is shown in figure 11, where the following patterns can be observed.

1) The monitoring points with a larger response is mainly the centroid of the rear camera, which is 20g@40Hz.

2) The Z-direction mechanical environment test is easy to pass for the front and rear cameras and the laser range finder. Although the input excitation is large, the relevant measuring points have weak response.

3) The response of the centroid of the two stereo mapping cameras and the laser range finder is not much different from that of their input surface.

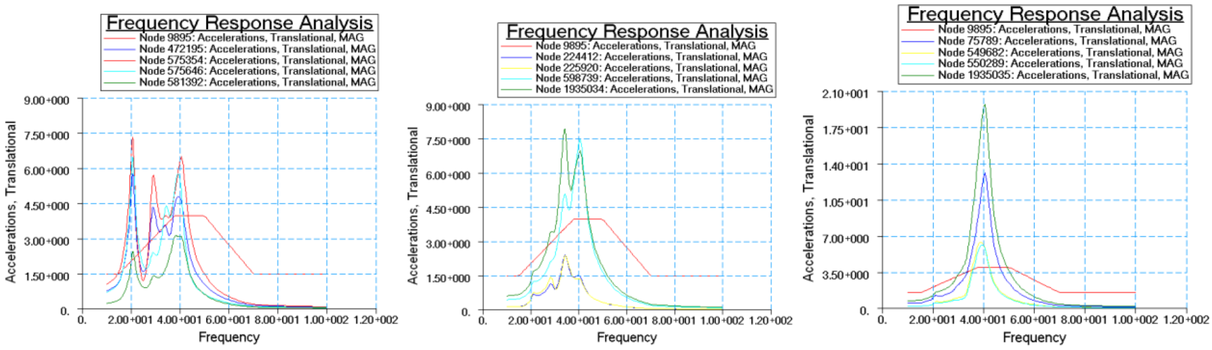

(a)Laser range finder (b) Front camera (c) Rear camera

Figure 11. Z-direction sinusoidal response cures

Thus, under the sinusoidal test conditions of X-,Y-, and Z-directions, the maximum peak response of the main optical instruments does not exceed 26g. This implies that the main frame of the system has an excellent structural stiffness. During the launching process, the main frame can provide an excellent mechanical environment for camera system without affecting its performance.

6. Conclusions

In this paper, the carbon fiber composite main frame is designed, which combines the advantages of high specific strength, low density, low expansion coefficient, and modified modulus of carbon fiber composites. The carbon fiber composite honeycomb panels, which constitute the main frame, consist of carbon fiber composite panels, aluminum honeycomb cores, and composite frames. The composite frame is made of composite rods and stiffeners connected by bonding titanium alloy joints. The simulation results show that the strength and stiffness of the main frame meet the requirements, and the design scheme is reasonable and feasible. The carbon fiber composite main frame has been applied to a particular type of remote sensor, which can provide new ideas for carbon fiber composite structure design of high-precision space optical instruments in the future.

References

[1] Sun G 2007 *J. Geomatic Science and Engineering*. **27** 46-51
[2] Miao J Y, Zhang L P and Tian T Y 2011 *J. Chinese Journal of Scientific Instrument*. **32** 2183-9
[3] Deng Y T, Li X and Yan F J 2015 *J. Spacecraft Recovery＆Remote Sensing*. **36** 86-91
[4] Liu Y, Xiao R Q and Han D D 2015 *J.Opt． Precision Eng.* **23** 3083-9
[5] Chen SH P 2003 *Design and Test of Space Camera (Munich)* (Beijing: Yu-hang Publishing Company) p 125
[6] Zhang J Q, Yan CH X 2009 *J. Chinese Journal of Optics and Applied Optics*. **2** 79-84
[7] Li W, Liu H W 2008 *J. Opt. Precision Eng*. **16** 2173-9
[8] Lin Z W, Liu Y Q, Liang Y 2007 *J. Opt.Precision Eng*. **18** 1181-5
[9] Li W, Guo Q F 2011 *J. Chinese Optics*. **4** 201-12
[10] Zhao Y, Li L 2011 *J. Spacecraft Recovery＆Remote Sensing*. **32** 68-74
[11] Jia ZH X, Jin G and Jia J Q 2011 *J. Chin. J. Space Sci*. **31** 395-400
[12] Guan Y J, Xin H W, Zhao G J 2008 *J. Chinese Journal of Optics and Applied Optics*. **15** 1157-63
[13] Wu J and Mao J J 2012 2*J. Spacecraft Recovery ＆ Remote Sensing*. **33** 34-41